## scientific reports



### **OPEN**

# Inhibition of Caspase-1-dependent pyroptosis alleviates myocardial ischemia/reperfusion injury during cardiopulmonary bypass (CPB) in type 2 diabetic rats

Wenjing Zhou¹,²,³, Yingya Yang¹,³, Zhouheng Feng², Yu Zhang², Yiman Chen¹, Tian Yu² & Haiying Wang¹⊠

Cardiovascular complications pose a significant burden in type 2 diabetes mellitus (T2DM), driven by the intricate interplay of chronic hyperglycemia, insulin resistance, and lipid metabolism disturbances. Myocardial ischemia/reperfusion (MI/R) injury during cardiopulmonary bypass (CPB) exacerbates cardiac vulnerability. This study aims to probe the role of Caspase-1-dependent pyroptosis in global ischemia/reperfusion injury among T2DM rats undergoing CPB, elucidating the mechanisms underlying heightened myocardial injury in T2DM. This study established a rat model of T2DM and compared Mean arterial pressure (MAP), heart rate (HR), and hematocrit (Hct) between T2DM and normal rats. Myocardial cell morphology, infarction area, mitochondrial ROS and caspase-1 levels, NLRP3, pro-caspase-1, caspase-1 p10, GSDMD expressions, plasma CK-MB, cTnI, IL-1β, and IL-18 levels were assessed after reperfusion in both T2DM and normal rats. The role of Caspase-1-dependent pyroptosis in myocardial ischemia/reperfusion injury during CPB in T2DM rats was examined using the caspase-1 inhibitor VX-765 and the ROS scavenger NAC. T2DM rats demonstrated impaired glucose tolerance but stable hemodynamics during CPB, while showing heightened vulnerability to MI/R injury. This was marked by substantial lipid deposition, disrupted myocardial fibers, and intensified cellular apoptosis. The activation of caspase-1-mediated pyroptosis and increased reactive oxygen species (ROS) production further contributed to tissue damage and the ensuing inflammatory response. Notably, myocardial injury was mitigated by inhibiting caspase-1 through VX-765, which also attenuated the inflammatory cascade. Likewise, NAC treatment reduced oxidative stress and partially suppressed ROS-mediated caspase-1 activation, resulting in diminished myocardial injury. This study proved that Caspase-1-dependent pyroptosis significantly contributes to the inflammation and injury stemming from global MI/R in T2DM rats under CPB, which correlate with the surplus ROS generated by oxidative stress during reperfusion.

**Keywords** Type 2 diabetes mellitus, Cardiopulmonary bypass, Myocardial ischemia/reperfusion injury, Pyroptosis, Caspase-1

The incidence of diabetes is on the rise, particularly among younger individuals. Global reports indicate that the global count of individuals aged 20–79 diagnosed with diabetes was 425 million in 2017, projected to escalate to 629 million by 2045¹. Type 2 diabetes (T2DM) constitutes over 90% of all diabetes cases. Among individuals aged 65 and above with T2DM, 70% succumb to cardiovascular ailments, a rate 2–4 times higher than their non-diabetic counterparts. Consequently, T2DM, serving as a significant risk factor for cardiovascular maladies, presents a substantial menace to worldwide public health.

<sup>1</sup>Department of Anesthesiology, Affiliated Hospital of Zunyi Medical University, 149 Dalian Street, Zunyi 563000, Guizhou, People's Republic of China. <sup>2</sup>Guizhou Key Laboratory of Anesthesia and Organ Protection, Affiliated Hospital of Zunyi Medical University, Zunyi 563003, Guizhou, People's Republic of China. <sup>3</sup>These authors contributed equally: Wenjing Zhou and Yingya Yang. <sup>∞</sup>email: wanghaiting-8901@163.com

Several studies demonstrate that T2DM patients undergoing cardiopulmonary bypass surgery (CPB) suffer more severe myocardial injury compared to non-diabetic counterparts. This heightened vulnerability is attributed to T2DM-induced metabolic dysregulation, exacerbating myocardial sensitivity to ischemia–reperfusion (I/R). Hyperglycemia, insulin resistance, and abnormal lipid metabolism typical in T2DM foster oxidative stress and inflammation, thereby worsening myocardial damage. In T2DM rat models, mitochondrial dysfunction triggers increased myocardial cell apoptosis, larger infarction areas, and more pronounced cardiac dysfunction, with necroptosis playing a pivotal role. Post-ischemia–reperfusion, T2DM patients exhibit elevated serum levels of inflammatory cytokines such as IL-1 $\beta$  and IL-6, which further amplify myocardial injury. Thus, strategies to mitigate myocardial I/R injury in T2DM patients are urgently needed to enhance their postoperative outcomes.

Numerous studies indicate that T2DM patients suffer more severe myocardial injury after cardiopulmonary bypass surgery (CPB) compared to non-diabetic individuals<sup>2,3</sup>. This susceptibility is linked to T2DM-related metabolic disruptions that increase myocardial sensitivity to ischemia–reperfusion (I/R). T2DM is typically associated with hyperglycemia, insulin resistance, and abnormal lipid metabolism, leading to oxidative stress and inflammation, which worsen myocardial damage<sup>4–6</sup>. In T2DM rat models, impaired myocardial mitochondrial function results in heightened myocardial cell apoptosis, larger infarction areas, and more severe cardiac dysfunction, with necroptosis playing a crucial role<sup>7</sup>. Following ischemia–reperfusion injury, T2DM patients exhibit significantly higher levels of inflammatory cytokines like IL-1 $\beta$  and IL- $\delta$  in their serum compared to healthy controls, further exacerbating myocardial injury<sup>8</sup>. Therefore, effective strategies are urgently needed to reduce myocardial ischemia/reperfusion injury in T2DM patients and improve their postoperative outcomes.

Cell pyroptosis is a programmed cell death mode triggered by caspase-1 or caspase-4/5/11 activation through the inflammasome pathway, leading to GSDM family-mediated inflammatory necrosis. Its hallmark feature is the formation of membrane pores, releasing inflammatory contents and initiating robust inflammatory responses  $^{9,10}$ . Recent studies underscore its role across various diseases, including cardiovascular, neurological, metabolic, and infectious disorders  $^{11-13}$ . Increased cell death-associated molecules in myocardial cells of T2DM rats link closely with diabetic cardiomyopathy, atherosclerosis, and coronary heart disease  $^{14-16}$ . In H9C2 myocardial cells under high glucose conditions, cell death exacerbates hypoxia/reoxygenation injuries  $^{17}$ . Diabetes-related complications also involve caspase-1-driven cell death in liver ischemia–reperfusion injury, aggravating hepatic dysfunction. Strategies targeting ROS and NLRP3 inflammasome activation show promise in mitigating liver I/R injury in diabetic patients  $^{18}$ . Activation of the NLRP3/caspase-1/IL-1 $^{18}$  pathway contributes significantly to renal tubular injury in diabetic nephropathy (DN). Inhibiting NLRP3 or caspase-1 expression deactivates inflammasomes, protecting renal tissue and suggesting a therapeutic target for DN treatment  $^{19}$ . Modulating the miR-214-3p/caspase-1 axis holds potential in reducing neuronal cell death, offering a strategy to mitigate diabetic brain damage  $^{20}$ .

During cell apoptosis, reactive oxygen species (ROS) serve as vital inflammatory signals, promoting NOD-like receptor protein 3 (NLRP3) activation via pathways like nuclear factor- $\kappa B$  (NF- $\kappa B$ ) and thioredoxin-interacting protein (TXNIP). This process plays a pivotal role in inducing cell apoptosis and fostering inflammatory responses 21,22. NLRP3 collaborates with apoptosis-associated speck-like protein (ASC) and procaspase-1, forming the NLRP3 inflammasome—a central component in cell apoptosis. This inflammasome significantly contributes to myocardial ischemia–reperfusion injury, where its activation triggers myocardial cell apoptosis and elicits inflammatory responses. Effective mitigation of myocardial ischemia–reperfusion injury and reduction of myocardial cell apoptosis can be achieved by inhibiting the caspase-1-dependent cell pyroptosis pathway, thus affording myocardial protection.

Hence, the intricate interconnection among myocardial ischemia–reperfusion injury, type 2 diabetes mellitus, and cell pyroptosis warrants thorough exploration. Unraveling their mechanisms and identifying corresponding therapeutic approaches holds paramount importance for preventing and managing associated disorders. This study delved into the involvement and potential mechanisms of caspase-1-dependent cell pyroptosis in T2DM rat models subjected to CPB-induced whole-heart ischemia–reperfusion injury.

#### Methods

#### Animal care and ethics statement

This study is reported in accordance with ARRIVE guidelines. All animal experiments were ethically approved by the Institutional Animal Care and Use Committee of Zunyi Medical University and were conducted following the guidelines outlined in the National Institutes of Health Guide for the Care and Use of Laboratory Animals. Adult male Sprague–Dawley rats (200–250 g) were procured from an authorized breeder and housed at the accredited Animal Center of Zunyi Medical University. The rats were accommodated in a controlled environment with a 12-h light/dark cycle, receiving standard rodent diet and unrestricted water access. They were housed in groups of four per cage, furnished with ample space and bedding material, and underwent a one-week acclimatization period prior to experimentation. The cages were maintained with daily cleaning routines, and the animals were continuously monitored for any signs of distress or illness throughout the experimental period.

#### Establishment of T2DM rat model

Adult male Sprague–Dawley rats, SPF grade, weighing approximately 300 g, were maintained on a standard diet for one week while monitoring their health status. Subsequently, they received a high-fat and high-sugar diet for four weeks. Following a 12-h fasting period, a 0.1% STZ solution was prepared and administered intraperitoneally at a dose of 35 mg/kg. Blood glucose levels were assessed after 72 h, and rats displaying blood glucose concentrations > 16.7 mmol/L were confirmed as T2DM rats. Model validation was further conducted through glucose tolerance testing.

#### **CPB** procedure

Following intraperitoneal injection of a 2% pentobarbital solution (50 mg/kg) for anesthesia, the rat was positioned supine on a board with its limbs and head secured.

Following the administration of pentobarbital, we assessed the depth of anesthesia by monitoring respiratory rate, heart rate, and reflex responses. Surgery was initiated only when the animals exhibited a complete loss of reflex responses and stable vital signs. Throughout the surgical procedure, animals were continuously monitored for signs of pain or distress, including changes in respiratory rate, heart rate, and reflex responses. Additional doses of anesthetic were administered if any signs of pain or awakening were observed. Utilizing a pediatric laryngoscope, tracheal intubation was achieved using a 16G catheter needle. Mechanical ventilation was initiated through connection to a small animal ventilator. A 26G catheter was inserted into the tail vein to facilitate continuous fluid infusion and drug administration. Cannulation of bilateral femoral arteries (22G) was performed; one side was linked to a real-time arterial blood pressure monitor, while the other served for blood reflux during CPB surgery. The right jugular vein was catheterized and positioned for optimal drainage. After catheter placement, a left sternal incision exposed the chest cavity, and the ascending aortic root was ligated following the third rib's excision. The rat's membrane oxygenator was connected to a blood reservoir and peristaltic pump. Before liver heparinization (4 mg/kg) via the tail vein, tubing was primed with a solution. Target flow rate, adjusted to attain 100 ml/kg·min-1, was continuously monitored alongside mean arterial pressure (MAP) and heart rate. Blood gas analysis was performed to ensure stable circulation and internal environment during CPB, maintaining MAP≥60 mmHg and Hct≥20%. Adjustments were made if MAP<60 mmHg, including increasing perfusion flow rate. The sham group experienced continuous circulation for 150 min post 10 min of simulated surgery, while the ischemia/reperfusion group maintained the target flow rate for 10 min before ascending aortic root clamping. After 30 min of cardiac arrest, temperature was gradually raised, the aorta opened, and circulation sustained for 120 additional minutes until experiment termination.

#### Temperature control during CPB

For inducing myocardial ischemia, ice chips were placed around the heart, simultaneously deactivating overhead light and the animal warming blanket, thereby reducing temperature to  $28-30\,^{\circ}$ C. Ice chips were removed and overhead light reinstated upon reperfusion initiation. Lab temperature was elevated, and the warming blanket activated to restore rectal temperature to  $32-34\,^{\circ}$ C.

#### Animal grouping

Nor+Sham (S) (n=18) and T2DM+S (n=18) Groups: The experiment terminates after 150 min of surgery with a target flow rate of 100 ml/kg·min-1.

 $\overline{\text{Nor+I/R}}$  (n = 18) and  $\overline{\text{T2DM+I/R}}$  (n = 18) Groups: Following a 10-min CPB period, the ascending aorta is clamped to induce 30 min of global cardiac ischemia. Subsequently, upon aortic release, the experiment concludes after 120 min of surgery.

T2DM+I/R+NAC (n = 18) and T2DM+I/R+Normal saline (NS) (n = 18) Groups: Prior to ischemia induction, NAC (150 mg/kg) or NS is continuously infused via the tail vein at a rate of 1 ml/h for 30 min. After a 10-min CPB interval, the ascending aorta undergoes clamping, leading to 30 min of global cardiac ischemia. The experiment culminates after 120 min of surgery upon aortic release.

T2DM+I/R+VX-765 (n = 18) and T2DM+I/R+DMSO (n = 18) Groups: VX-765 (16 mg/kg) or DMSO (0.5 ml/kg) is injected into the abdominal cavity 30 min prior to ischemia induction. After 10 min of CPB, the ascending aorta experiences clamping, inducing 30 min of global cardiac ischemia. Subsequently, upon aortic release, the experiment concludes after 120 min of surgery.

In our experiment, there were eight groups, with each group consisting of 18 rats for the electron microscopy (n=6), infarct size (n=6), and protein quantification experiments (sharing the same heart sample with the immunofluorescence experiment) (n=6). Therefore, the study required a total of 36 normal rats and 108 T2DM rats. The mortality rate for normal rats undergoing CPB-I/R modeling was 5.56%, while the mortality rate for T2DM rats was 12.04%. If a rat died during the modeling process, an additional rat was included to maintain the sample size.

#### Myocardial infarction size assessment

The extent of myocardial infarction was determined employing the TTC (2,3,5-triphenyltetrazolium chloride) staining method. A 1% TTC staining solution was prepared and prewarmed to 37 °C in a light-resistant water bath prior to application. Upon experiment completion, intact rat hearts were promptly excised and placed in pre-cooled 4 °C PBS buffer. Following drainage of residual blood from the heart chambers, hearts were dried with blotting paper, then cooled at -80 °C for 12 min.

Subsequently, hearts were sectioned into five uniformly thick segments across the heart's cross-section. These sections were then incubated in a pre-warmed TTC dye solution at room temperature (37 °C) for 30 min. After incubation, heart sections were rinsed with PBS, blotted with absorbent paper, and gently shaped before being fixed in formalin for 24 h and subsequently photographed. Image J software facilitated the calculation of the myocardial infarction area, presented as a percentage of the total area to depict the extent of myocardial infarction.

#### Transmission electron microscopy

In this study, transmission electron microscopy (TEM) was employed to investigate the ultrastructure of left ventricular myocardial tissue in rats. The tissue was initially fixed in 2.5% glutaraldehyde, followed by post-fixation with 1% osmium tetroxide. Subsequent steps included dehydration through an ethanol gradient, embedding in epoxy resin, and sectioning into thin slices using an ultramicrotome. These sections were stained with uranyl

acetate and lead citrate prior to examination with a transmission electron microscope. Through this process, various ultrastructural changes were observed and analyzed, encompassing modifications in mitochondrial morphology, myofibril structure, and the identification of cellular damage indicators like swelling or vacuolation.

#### Flameng score

The Flameng score stands as a widely accepted approach for quantifying mitochondrial impairment within cardiac tissue. This method holds significance as a tool to gauge the extent of myocardial injury across diverse cardiac conditions. An experienced electron microscopist, unaware of the experimental contexts and treatment groups, is tasked with determining the score. This measure is employed to ensure both objectivity and precision in assessment. The employed Flameng score variant adheres to a 0–4 grading system:

Score 0: Normal mitochondrial configuration, characterized by orderly cristae and intact outer and inner membranes

Score 1: Minimal mitochondrial impairment, marked by slightly disorganized cristae and/or minor swelling or vacuolization.

Score 2: Mild to moderate mitochondrial damage, indicating moderately disrupted cristae and/or moderate swelling or vacuolization.

Score 3: Moderate to severe mitochondrial damage, showcasing severely disrupted cristae and/or pronounced swelling or vacuolization.

Score 4: Severe mitochondrial damage, manifesting as complete cristae disruption and/or fragmentation of the mitochondrial matrix.

#### Myocardial ROS assessment

Upon reperfusion completion, left ventricular myocardial tissue was collected and embedded using OTC embedding solution. Subsequently, the myocardial tissue was sectioned into 10-µm-thick segments using a frozen microtome. These sections were directly affixed to slides. To initiate the assessment, the sections underwent three 5-min washes with pre-warmed PBS at 37 °C. A 10 µmol/l solution of DHE probe, similarly warmed to 37 °C, was then applied onto the sections. The sections were incubated within a light-resistant humidified chamber at 37 °C for 30 min. Following the incubation period, three additional washes with PBS at 37 °C (5 min each) were executed under light-protected conditions. Post-washing, the sections were allowed to dry before being treated with DAPI dye and enclosed with coverslips. The sections were subsequently examined and imaged using fluorescence microscopy. Utilizing Image J software, the average fluorescence intensity was assessed and recorded.

#### Quantification of myocardial Caspase-1 immunofluorescence

The tissue sections were initially fixed using 1.4% paraformaldehyde for a 15-min duration. Subsequent steps involved sequential washes with PBS to enhance cell membrane permeability: incubation with 0.2% Triton X-100 for 10 min, followed by three PBS washes, each lasting 5 min. For primary antibody application, a dropwise addition of diluted primary antibody was performed, and refrigeration was maintained overnight at 4 °C. The sections were subsequently washed three times with PBS for 15 min each time. After preparing and applying the secondary antibody, sections were placed in a humid chamber for a 1-h incubation at room temperature. This was followed by three PBS washes, each lasting 15 min. Upon completing these procedures, the sections underwent observation and photography via fluorescence microscopy.

For each heart, 5–6 images were captured and analyzed to ensure comprehensive coverage and accurate representation of the tissue. Each heart was sectioned into several regions: apex, mid-ventricle, and base. From each section, images were taken from both the endocardial and epicardial regions. This systematic approach ensured that different areas of the myocardium were represented, capturing the heterogeneity within the heart tissue. The images were analyzed using ImageJ software to quantify fluorescence intensity. The mean fluorescence intensity for each image was calculated. These values were then averaged to obtain a single representative value for each heart, which was used for statistical analysis. This process was performed separately for both ROS and caspase-1 immunofluorescence measurements.

#### Western blot analysis

Rat left ventricular myocardial tissue samples were collected and homogenized in RIPA buffer supplemented with protease inhibitors. The protein content was quantified utilizing the Bradford assay, and equivalent protein quantities were loaded onto a 10% SDS-polyacrylamide gel for electrophoresis. Following gel electrophoresis, proteins were transferred onto a PVDF membrane, which was then subjected to a 1-h blocking step at room temperature using 5% non-fat milk. Subsequently, primary antibodies ( $\beta$ -Actin: Affinity, AF7018, 1:5000; NLRP3: Affinity, DF7438, 1:1000; GSDMD: Affinity, DF12275, 1:1000; por-Caspase1: Affinity, AF5418, 1:1000; Caspase p10: Affinity, AF4022, 1:500) specific to the protein of interest within rat left ventricular myocardial tissue were employed for an overnight incubation at 4 °C. This was followed by a 1-h incubation at room temperature with a secondary antibody (Goat Anti-Rabbit IgG(H+L) HRP: MULTI SCIENCES, GAR0072, 1:0000) conjugated to horseradish peroxidase. The PVDF membrane was subsequently processed using an enhanced chemiluminescence system and analyzed through chemiluminescence detection. Protein expression levels were quantified via densitometric analysis performed using ImageJ software. To ensure reliability, the experiments were conducted in triplicate using distinct samples. Due to budget constraints and in an effort to conserve antibodies, the blots were trimmed before hybridization with antibodies. Images of all blots with membrane edges visible were included in the Supplementary Information file.

#### Blood sample collection and ELISA assay

Heparinized tubes were employed to collect blood samples from experimental animals, subsequently centrifuged at 1500 g for 10 min at 4 °C, yielding plasma. The concentrations of cardiac enzymes, encompassing creatine kinase-MB (CK-MB) and lactate dehydrogenase (LDH), alongside inflammatory cytokines such as tumor necrosis factor-alpha (TNF-a) and interleukin-6 (IL-6), were determined via commercially available ELISA kits (BioLegend, San Diego, CA, USA) following the manufacturer's guidelines. The procedure involved the coating of 96-well plates with specific capture antibodies corresponding to each target molecule, left to incubate overnight at 4 °C. After buffer washing, the plates were blocked with 1% bovine serum albumin (BSA) for 1 h at room temperature. Subsequent steps included addition of plasma samples and standard solutions into the wells, followed by a 2-h incubation at room temperature. The wells were then subjected to a sequence of washing and incubation with biotinylated detection antibodies for 1 h at room temperature. Streptavidin-horseradish peroxidase (HRP) conjugate was applied for a 30-min incubation, followed by a final washing step. The plates were developed using 3,3',5,5'-tetramethylbenzidine (TMB) substrate, and absorbance was quantified at 450 nm using a microplate reader. Quantification of cardiac enzymes and cytokines relied on a standard curve generated from known protein concentrations. All samples were analyzed in duplicate, and mean values were derived. The intra-assay and inter-assay coefficients of variation (CVs) were both less than 10% and 15%, respectively, indicative of robust assay precision.

#### Statistical analysis

GraphPad Prism version 8.0.2 (GraphPad Software, La Jolla, CA, USA) was employed to analyze data from Western blot findings, immunofluorescence intensity, myocardial infarction area, mitochondrial Flameng score, heart rate, blood pressure, and temporal hemoglobin alterations. Prior to analysis, normality was assessed via the Shapiro–Wilk test, and homogeneity of variances was determined using Levene's test. For comparative analyses, the unpaired Student's t-test was employed when comparing two groups, while one-way ANOVA followed by Tukey's multiple comparison test was utilized for comparisons involving more than two groups. Outcomes are presented as mean  $\pm$  standard error of the mean (SEM). Statistical significance was denoted at a level of P < 0.05.

#### Results

### The hemodynamic and internal environment effects of global MI/R in a cardiopulmonary bypass model of T2DM rats

Figure 1A, B displays the outcomes of glucose tolerance tests (IPGTT & OGTT). Following the administration of a 20% glucose solution via gavage or intraperitoneal injection, both normal and T2DM rats exhibited a substantial increase in blood glucose levels, which gradually decreased after 30 min. Remarkably, T2DM rats consistently displayed higher blood glucose levels exceeding 16.7 mmol/l (P < 0.05) compared to normal rats, indicating impaired glucose tolerance and confirming the effectiveness of the model. Mean arterial pressure (MAP) in all groups demonstrated a gradual decrease over time, remaining above 60 mmHg at all time points. Compared to the T0 group, T1–T4 groups exhibited significant decreases in MAP (P < 0.05) (Fig. 1C). Similarly, Fig. 1D reveal that heart rate (HR) significantly decreased in T1-T4 groups compared to the T0 group (P < 0.05). The I/R groups all achieved complete cardiac arrest at T2 and were successfully resuscitated at T3, approaching the S group at T4. Figure 1E illustrate that the hematocrit (Hct) of all groups remained above 20% at all time points, despite a significant decrease at T1 compared to T0 (P < 0.05) due to the dilution effect of the priming solution. Overall, these findings confirm the stable hemodynamics and internal environment of T2DM rats and normal rats during CPB.

## The severity of myocardial ischemia/reperfusion injury was greater in T2DM rats compared to normal rats

The infarct area was found to be larger in both the Nor+I/R and T2DM+I/R groups compared to their respective S group (P < 0.05), as determined through TTC staining. Furthermore, the T2DM+I/R group exhibited a significantly greater infarct area than the Nor+I/R group during the ischemia/reperfusion (I/R) state (P < 0.05), as depicted in Fig. 2A, B, indicating a more severe local myocardial injury. The application of ELISA facilitated the detection of cardiac enzymes CK-MB and cTnI release within rat plasma. The release of both CK-MB and cTnI was notably elevated in the T2DM+S group when contrasted with the Nor+S group (P < 0.05). Similarly, the release of CK-MB and cTnI was markedly higher in both the Nor+I/R and T2DM+I/R groups compared to their corresponding S group (P < 0.05). In particular, the T2DM+I/R group displayed a notably higher release of CK-MB and cTnI than the Nor+I/R group in the I/R state (P < 0.05), as illustrated in Fig. 2C, D.

The ultrastructure of cardiac myocytes was examined using transmission electron microscopy (Fig. 2E). Subsequent to global ischemia/reperfusion induced by CPB, both the Nor+I/R and T2DM+I/R groups exhibited myocardial fiber disorder, breakage, and interstitial edema. Upon higher magnification, the Nor+S group displayed regular mitochondrial morphology with few instances of rupture. Conversely, the Nor+I/R and T2DM+I/R groups presented the disappearance of mitochondrial ridges, loss of mitochondrial membrane integrity, and mitochondrial swelling and rupture, highlighting severe local cellular damage and compromised myocardial integrity. These alterations were accompanied by early indicators of cell death, including nuclear swelling and chromatin marginalization. The evaluation of mitochondrial scoring, as shown in Fig. 2F, unveiled a notably higher mitochondrial score in the T2DM+S group compared to the Nor+S group (P<0.05). Furthermore, substantial mitochondrial damage was evident in both the Nor+I/R and T2DM+I/R groups, reflected by an increased mitochondrial score compared to their corresponding S groups (P<0.05). Notably, the T2DM+I/R group exhibited more severe mitochondrial damage than the Nor+I/R group during the I/R state (P<0.05), indicating a critical local response to ischemia–reperfusion injury.

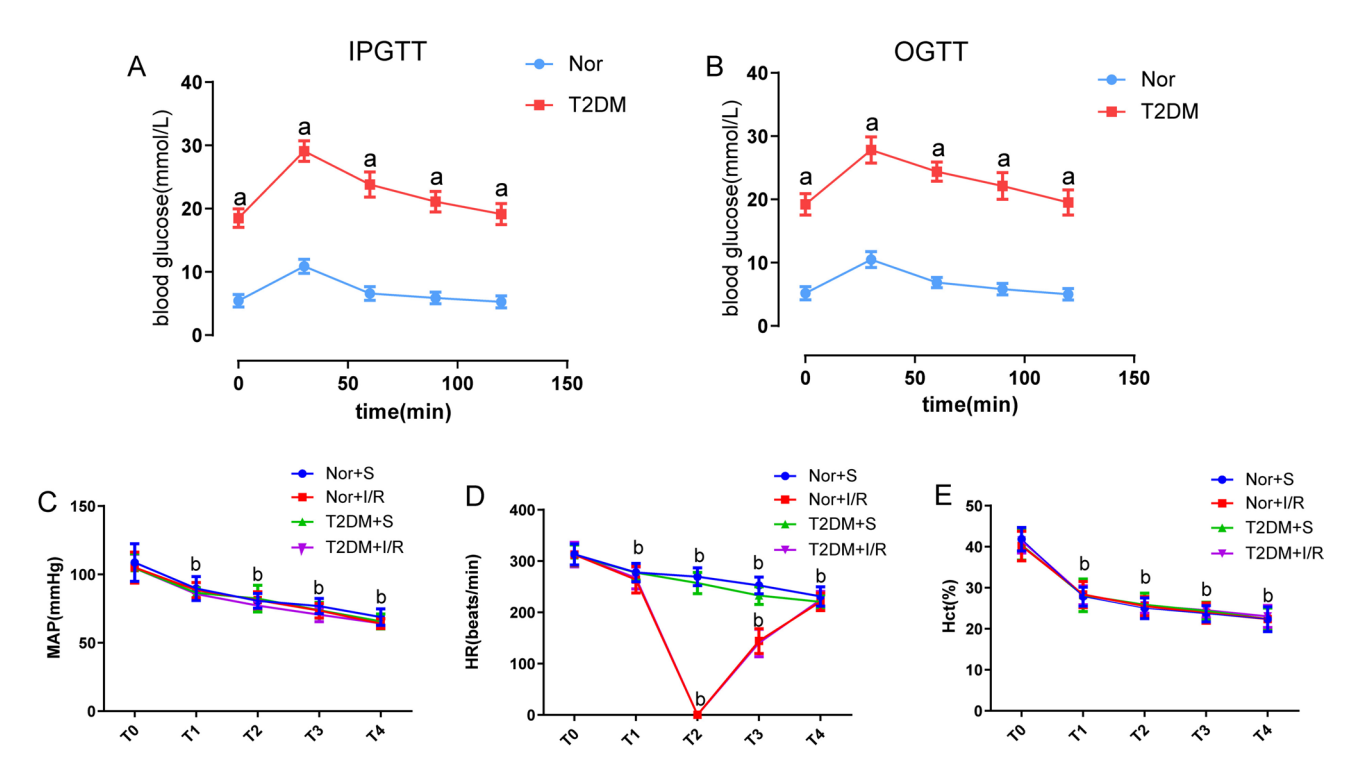


Fig. 1. T2DM rats and normal rats exhibit same changes in hemodynamics and internal environment during CPB. (A) Blood glucose level in intraperitoneal glucose tolerance test (IPGTT). (B) Blood glucose level in oral glucose tolerance tests (OGTT). (C) Changes in Mean Arterial Pressure (MAP) among different groups of rats. (D) Changes in heart rate (HR) among different groups of rats. The heart rate (HR) and blood pressure are monitored via the femoral artery rather than electrocardiography. The observed drop in HR to zero in the control group occurs during aortic cross-clamping, when the heart temporarily ceases to eject blood. This is an artifact of the monitoring method and not an indication of actual cardiac arrest. (E) Changes in hematocrit (Hct) among different groups of rats. Compared with the Nor group, a represents P < 0.05. Compared to the T0 time point within the same group, b indicates P < 0.05.

## The extent of cellular apoptosis activation in T2DM rats subjected to CPB-induced global ischemia/reperfusion surpassed that observed in normal rats

Reactive oxygen species (ROS) production was evaluated through fluorescence microscopy employing DHE and DAPI staining (Fig. 3A, B). The outcomes revealed heightened ROS generation in T2DM+S rats in comparison to Nor+S rats (P < 0.05). Moreover, both Nor+I/R and T2DM+I/R rats exhibited elevated ROS production relative to their respective S groups (P < 0.05). Notably, during the I/R state, T2DM+I/R rats displayed a more pronounced rise in ROS production than Nor+I/R rats (P < 0.05), contributing to further myocardial damage and dysfunction. Immunofluorescence staining was utilized to assess the relative fluorescence intensity of caspase-1 (Fig. 3C, D. Findings demonstrated escalated caspase-1 expression in T2DM+S rats compared to Nor+S rats (P < 0.05). Similarly, both Nor+I/R and T2DM+I/R rats displayed heightened caspase-1 expression in contrast to their corresponding S groups (P < 0.05). Remarkably, in the I/R state, T2DM+I/R rats exhibited a more substantial upsurge in caspase-1 expression than Nor+I/R rats (P < 0.05), indicating enhanced local inflammation and pyroptosis, exacerbating myocardial injury.

Western blot analysis unveiled augmented expression of NLRP3, pro-caspase-1, caspase-1 p10, and GSDMD across all groups relative to Nor+S rats (P < 0.05) (Fig. 4A–E). ELISA results (Fig. 4F, G) indicated amplified release of IL-1 $\beta$  and IL-18 in T2DM+S rats compared to Nor+S rats (P < 0.05). Furthermore, both Nor+I/R and T2DM+I/R rats showed increased release of IL-1 $\beta$  and IL-18 in comparison to their corresponding S groups (P < 0.05). Notably, T2DM+I/R rats displayed a more pronounced elevation in release of IL-1 $\beta$  and IL-18 compared to Nor+I/R rats during the I/R state (P < 0.05), reflecting extensive local myocardial damage and systemic inflammatory response.

#### Inhibiting caspase-1 activation mitigates myocardial injury in T2DM rats with MI/RI

We then used the caspase-1 inhibitor VX-765 to assess the impact of caspase-1 inhibition on MI/RI-induced myocardial injury in T2DM rats. VX-765 is a prodrug that requires activation by cellular esterases to convert into its active form, VRT-043198, which effectively inhibits caspase-1 $^{23}$ . Due to this requirement, VX-765 (16 mg/kg) was dissolved in DMSO (0.5 ml/kg DMSO diluted with NS to 0.9 ml) and administered intraperitoneally 30 min before ischemia to ensure its conversion to the active form prior to myocardial I/R injury. This method allows sufficient time for the prodrug to be activated within the target cells. The T2DM+I/R+VX-765 group displayed a smaller myocardial infarction area, in contrast to the control group (P<0.05) (Fig. 5A). Transmission electron

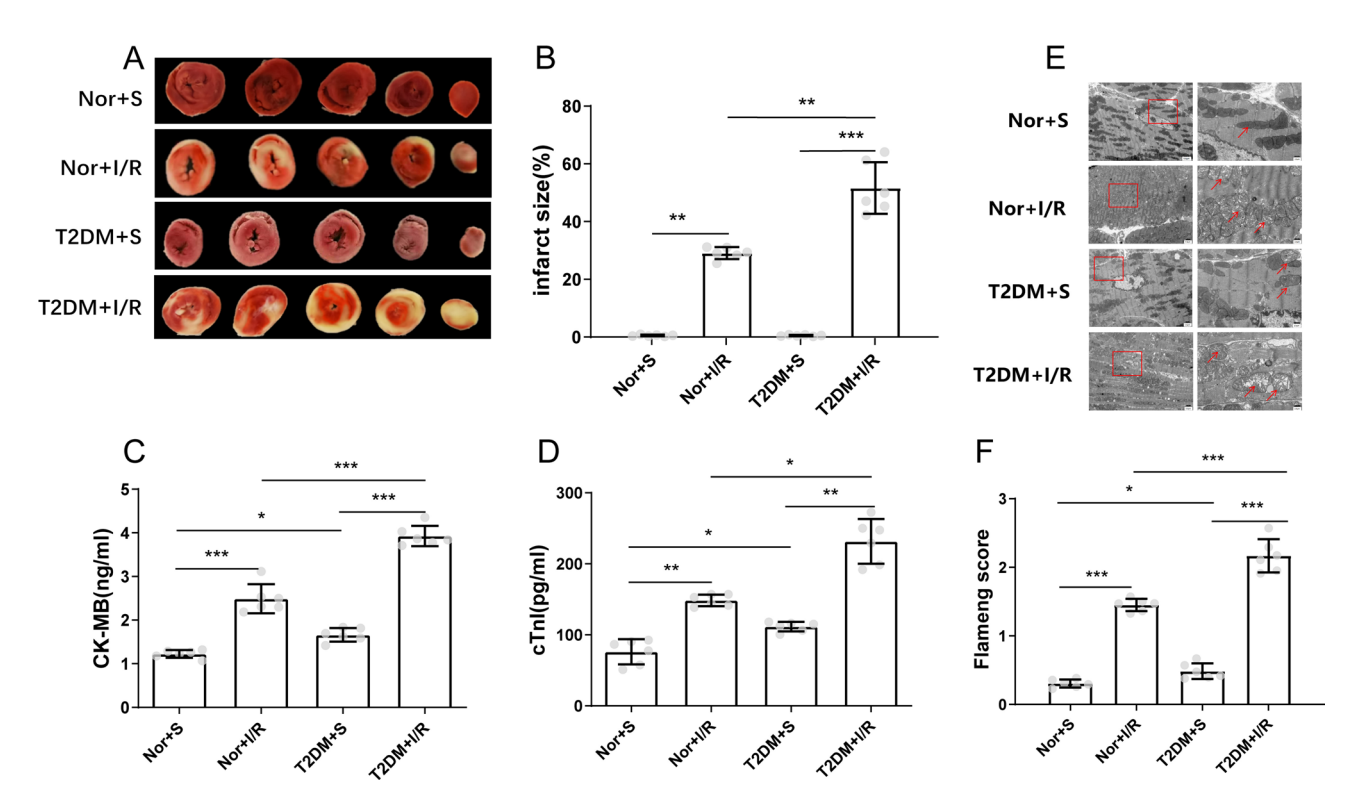


Fig. 2. Myocardial injury following global ischemia/reperfusion in T2DM rats and normal rats. (A) Comparison of infarct area in rat hearts after TTC staining among different groups, where the white area represents the myocardial infarct region and the red area represents the normal myocardial region. (B) Statistical results of Myocardial infarct area in different groups of rats. (C) and (D) ELISA detection results of myocardial enzymes (ck-mb, ctni) in different groups of rats. (E) Transmission electron micrograph of cardiac tissue, with the enlarged view of the red-framed area on the left shown on the right side. The arrows indicate damaged mitochondria. (F) Statistical results of myocardial mitochondrial scoring in different groups of rats.  $^*P < 0.05, ^*P < 0.01, ^**P < 0.001$ .

microscopy depicted disorganized and swollen myocardial fibers across all groups, with varying mitochondrial damage; however, the T2DM+I/R+VX-765 group exhibited notably reduced mitochondrial impairment (P < 0.05) (Fig. 5B). The caspase-1 inhibitor VX-765 significantly attenuated caspase-1 activation and downregulated its downstream targets, p10 and GSDMD (P < 0.05), while NLRP3 and pro-caspase-1 expression remained unaffected (Fig. 5C–G). Moreover, ELISA analysis of plasma samples revealed diminished levels of IL-1 $\beta$  and IL-18 in the T2DM+I/R+VX-765 group, along with decreased CK-MB and cTnI levels, compared to the control group (P < 0.05) (Fig. 5H–K). These results imply that caspase-1 inhibition might mitigate myocardial injury in T2DM rats during MI/RI, potentially by suppressing the inflammasome activation pathway.

## ROS induction significantly contributes to cell apoptosis during myocardial ischemia/reperfusion injury in T2DM rats

N-acetylcysteine (NAC) was employed to mitigate reactive oxygen species (ROS) in myocardial cells. The relative ROS fluorescence intensity in T2DM+I/R+NAC myocardial tissue notably decreased compared to the control group (P < 0.05), indicating effective ROS reduction by NAC in T2DM+I/R+NAC rat myocardial cells (Fig. 6A, B). Furthermore, caspase-1 expression in T2DM+I/R+NAC myocardial tissue significantly decreased compared to the control group (P < 0.05), as indicated by relative caspase-1 fluorescence intensity among groups (Fig. 6C, D).

Myocardial infarction area in T2DM+I/R+NAC rats was notably smaller than in the control group (P < 0.05), as indicated in Fig. 7A. Transmission electron microscopy images of myocardial tissue revealed disordered myocardial fiber arrangement, interstitial edema, rupture, and varying degrees of mitochondrial damage including mitochondrial ridge disappearance, loss of mitochondrial membrane integrity, and swelling. The mitochondrial injury score illustrated significantly reduced mitochondrial damage in the T2DM+I/R+NAC group versus the control group (P < 0.05) (Fig. 7B). The T2DM+I/R+NAC rat myocardial tissue exhibited markedly diminished expression of NLRP3, pro-caspase-1, caspase-1 p10, and GSDMD compared to the control group (P < 0.05), as presented in Fig. 7C–G. ELISA outcomes demonstrated considerable reduction in plasma IL-1 $\beta$  and IL-18 levels, and significantly reduced release of CK-MB and cTnI in T2DM+I/R+NAC rats compared to the control group (P < 0.05), as detailed in Fig. 7H–K.

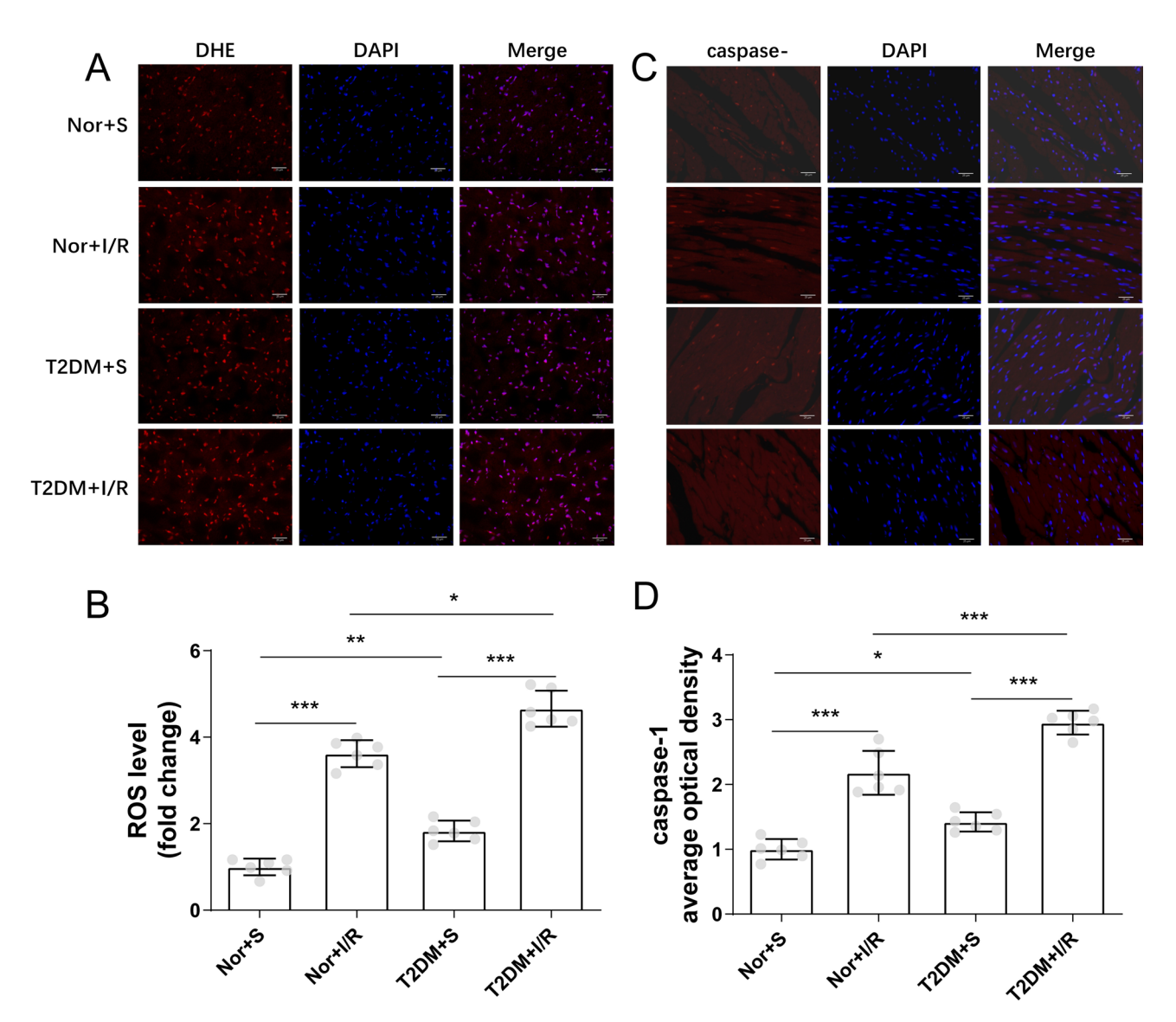


Fig. 3. The oxidative stress response following CPB in T2DM rats and normal rats. (A) Rat myocardial tissue ROS immunofluorescence staining images for each group, with red fluorescence representing ROS and blue fluorescence representing cell nuclei. (B) Statistical results of relative ROS fluorescence intensity in rat myocardial tissue for each group. (C) Rat myocardial tissue caspase-1 immunofluorescence staining images for each group, with red fluorescence representing caspase-1 and blue fluorescence representing cell nuclei. (D) Statistical results of relative caspase-1 fluorescence intensity in rat myocardial tissue for each group. \*P < 0.05, \*P < 0.01, \*\*P < 0.001.

#### Discussion

This study investigated the impact of global myocardial ischemia/reperfusion (MI/R) on hemodynamics and the internal milieu within a cardiopulmonary bypass (CPB) model using type 2 diabetes mellitus (T2DM) rats. Our findings revealed that T2DM rats exhibited impaired glucose tolerance but maintained stable hemodynamics and internal conditions during CPB. However, T2DM rats experienced heightened myocardial ischemia/reperfusion injury compared to normal rats. This was evident through substantial lipid deposition, disrupted myocardial fibers, fragmentation, and interstitial edema, which underscores the exacerbated local myocardial injury and critical local cellular damage due to T2DM-mediated metabolic disturbances. Moreover, the activation of cellular apoptosis was significantly more pronounced in T2DM rats during CPB-induced global ischemia/reperfusion, accompanied by elevated generation of reactive oxygen species and increased caspase-1 expression. Notably, the marked increase in ROS levels in the myocardial tissue of T2DM rats highlights the local oxidative stress contributing to myocardial injury. Elevated caspase-1 expression suggests enhanced local inflammation and cell death via pyroptosis, further aggravating myocardial damage. The significantly higher levels of cardiac enzymes (CK-MB and LDH) and inflammatory cytokines (TNF- $\alpha$  and IL-6) in T2DM rats indicate extensive local myocardial damage and a pronounced systemic inflammatory response. Thus, T2DM rats subjected to CPB-induced global cardiac ischemia/reperfusion displayed exacerbated myocardial tissue damage and inflammatory

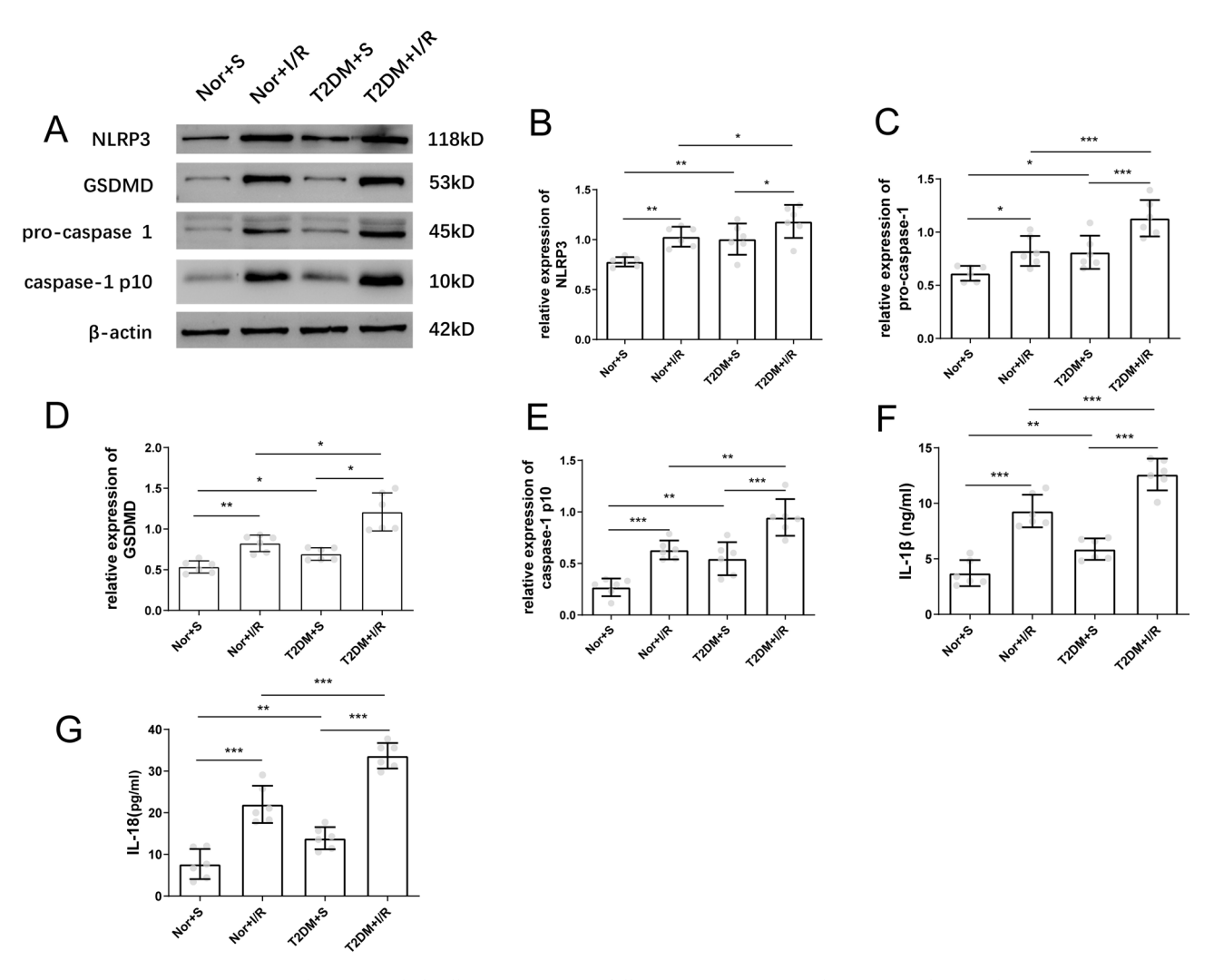


Fig. 4. The myocardial cell apoptosis status following CPB in rats with T2DM and normal rats. (A) Representative Western blot bands of apoptosis-related proteins in rat myocardial tissue from each group. (B–E) Statistical results of expression levels for each apoptosis-related protein. (F) and (G) Statistical results of ELISA measurements for IL-1 $\beta$  and IL-18 levels in rat groups. \*P<0.05, \*\*P<0.01, \*\*\*P<0.001.

responses, possibly due to heightened cell necroptosis activation, potentially linked to excessive ROS production during reperfusion.

This investigation establishes that type 2 diabetes mellitus (T2DM), accompanied by metabolic syndrome, involving chronic hyperglycemia, insulin resistance, and lipid metabolism disorders, heightens not only the vulnerability to myocardial ischemia and cardiomyopathy but also diminishes the innate myocardial safeguards and tolerance against ischemia/reperfusion (I/R) injury. Consequently, this cascade contributes to the development of heart failure and sudden cardiac death<sup>24</sup>.

In this study, by utilizing transmission electron microscopy to scrutinize myocardial tissue, we identified substantial lipid deposition within myocardial cells of T2DM rats. However, these rats exhibited no pathological changes indicative of diabetic cardiomyopathy (DCM), such as interstitial fibrosis or myocardial remodeling, when compared to normal rats<sup>25,26</sup>. Conversely, T2DM+S rats displayed intensified mitochondrial damage in comparison to Nor+S rats. This heightened damage can be ascribed to various pathways, including the chronic hyperglycemia-induced advanced glycation end products (AGEs) pathway, the protein kinase C (PKC) pathway, and heightened mitochondrial metabolism. These factors contribute to the accumulation of mitochondrial reactive oxygen species (ROS), alterations in respiratory function and membrane potential, ultimately culminating in mitochondrial dysfunction<sup>27</sup>.

The study successfully established the T2DM model, confirmed through subsequent transmission electron microscopy analysis, which unveiled significant pathological alterations in the mitochondria of T2DM+S rats. These modifications encompassed mitochondrial swelling, cristae disappearance, and a higher score of mitochondrial injury. These findings signify that the T2DM-associated metabolic syndrome can trigger myocardial mitochondrial dysfunction even before the conventional pathological manifestations of DCM, like interstitial fibrosis and myocardial remodeling. Moreover, the T2DM+S cohort demonstrated heightened expression of cell apoptosis-related proteins and the release of inflammatory factors in comparison to the Nor+S group. This observation implies that T2DM itself possesses the potential to activate cell apoptosis.

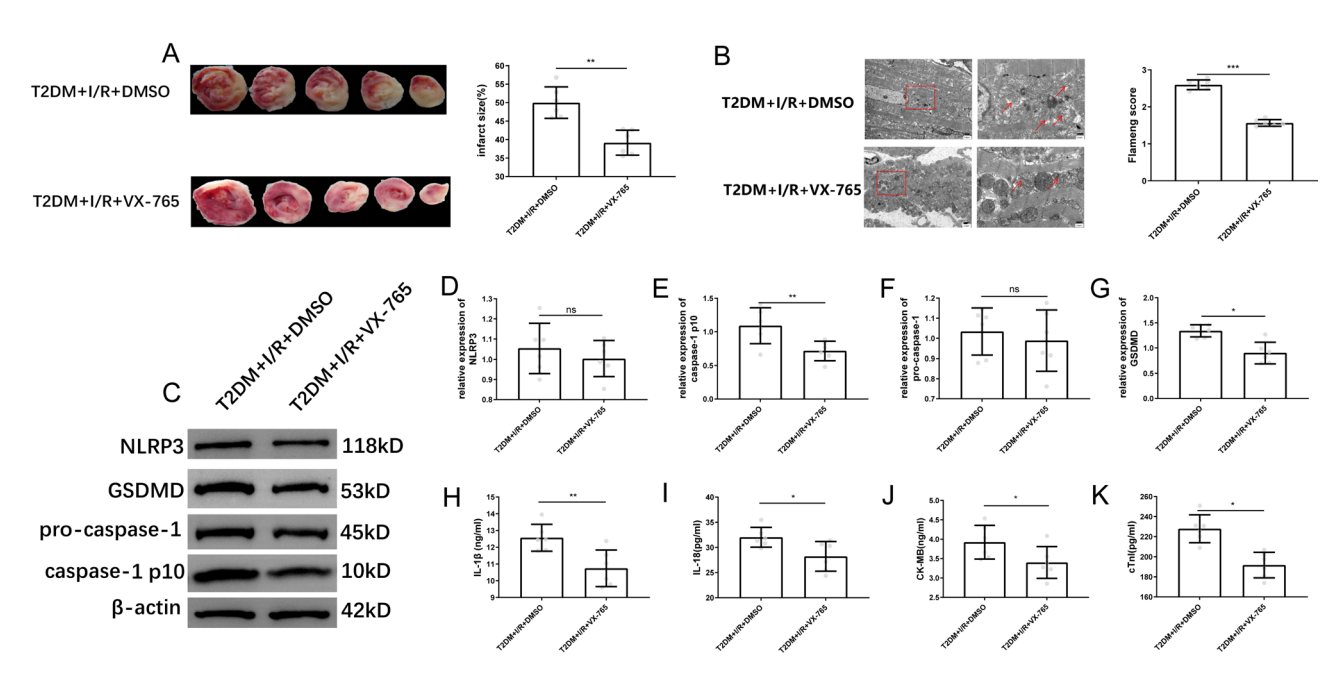


Fig. 5. Inhibiting caspase-1 can alleviate myocardial damage in CPB-induced cardiac injury in T2DM rats. (A) Comparison of myocardial infarction areas between the VX-765 treatment group and the non-treatment group in rats. (B) Transmission electron micrograph of cardiac tissue, with the enlarged view of the red-framed area on the left shown on the right side. The arrows indicate damaged mitochondria, and statistical results of myocardial mitochondrial scoring. (C) Representative Western blot bands of apoptosis-related proteins. (D-G) Statistical results of expression levels for each apoptosis-related protein. (H-K) Statistical results of ELISA measurements for IL-1 $\beta$ , IL-18, CK-MB and cTnI levels. \*P<0.05, \*\*P<0.01, \*\*\*P<0.001.

Caspase-1-dependent pyroptosis represents a mode of cell demise triggered by caspase-1 activation in response to heightened reactive oxygen species (ROS) levels  $^{28,29}$ . This investigation revealed a substantial elevation in the expression of pyroptosis-associated proteins—NLRP3, pro-caspase-1, caspase-1 p10, and GSDMD—alongside the release of inflammatory cytokines IL-1 $\beta$  and IL-18 across all rat groups. Particularly, in comparison to their respective "S" groups, both the Nor+I/R and T2DM+I/R groups exhibited heightened protein expression. Notably, the T2DM+I/R group demonstrated a more pronounced increase, indicating an escalated activation of caspase-1-dependent pyroptosis, thereby culminating in heightened inflammatory damage. In our study, we observed an increase in the inactive form of caspase-1 in the ischemia–reperfusion (I/R) groups (Fig. 4). This finding may be attributed to the early initiation of inflammasome activation during the ischemic phase induced by CPB. It is hypothesized that the accumulation of inactive caspase-1 forms part of the preparatory phase for subsequent inflammatory responses during reperfusion. This phenomenon has been supported by previous studies suggesting that inflammasome components, including caspase-1, undergo initial accumulation and activation under ischemic conditions  $^{30,31}$ . Therefore, the observed increase in inactive caspase-1 forms in our study underscores the complex interplay between ischemia and subsequent inflammatory cascades in myocardial ischemia–reperfusion injury.

VX-765, an extensively selective and safe caspase-1 inhibitor, is a bioavailable small molecule that underwent testing in a phase II human clinical trial for epilepsy treatment<sup>32</sup>. Notably, it effectively diminishes plasma IL-1 $\beta$  and IL-18 levels, exhibiting anti-inflammatory effects across diverse disease processes. Despite its demonstrated efficacy, the exact mechanism of action remains enigmatic<sup>33,34</sup>. To effectively inhibit caspase-1, VX-765 must undergo enzymatic conversion to VRT-043198. In this study, 16 mg/kg of VX-765 was dissolved in DMSO (0.5 ml/kg DMSO+NS diluted to 0.9 ml) and administered intraperitoneally 30 min before ischemia to ensure its transformation into its active form prior to myocardial I/R<sup>35</sup>.

The results demonstrate that VX-765 effectively mitigated myocardial injury in T2DM rats subjected to global ischemia/reperfusion (I/R). VX-765 restrained caspase-1 activation, leading to reduced expression of caspase-1 p10 fragment and downstream GSDMD. This, in turn, caused a decrease in the release of IL-1 $\beta$  and IL-18, while leaving the expression of upstream proteins NLRP3 and pro-caspase-1 unaffected. The T2DM+I/R+VX-765 group exhibited noteworthy reductions in mitochondrial score, myocardial infarct size, and the release of CK-MB and cTnI when compared to the T2DM+I/R+DMSO control group. These findings underscore the pivotal role of caspase-1-mediated cell pyroptosis in the inflammatory and injurious progression of I/R injury in T2DM rats. Inhibition of caspase-1 activation through VX-765 emerges as a viable approach for safeguarding ischemic/reperfused myocardium.

Under normal physiological conditions, the mitochondrial respiratory chain minimally converts oxygen into reactive oxygen species (ROS). However, metabolic alterations in type 2 diabetes (T2DM) individuals, such as adipocyte hypertrophy, hypoxia, chronic hyperglycemia, and insulin resistance, activate the advanced glycation end product (AGE) and protein kinase C (PKC) pathways. These changes culminate in ROS accumulation within mitochondria, disrupting the balance between oxidation and antioxidation. This, in turn, triggers mitochondrial

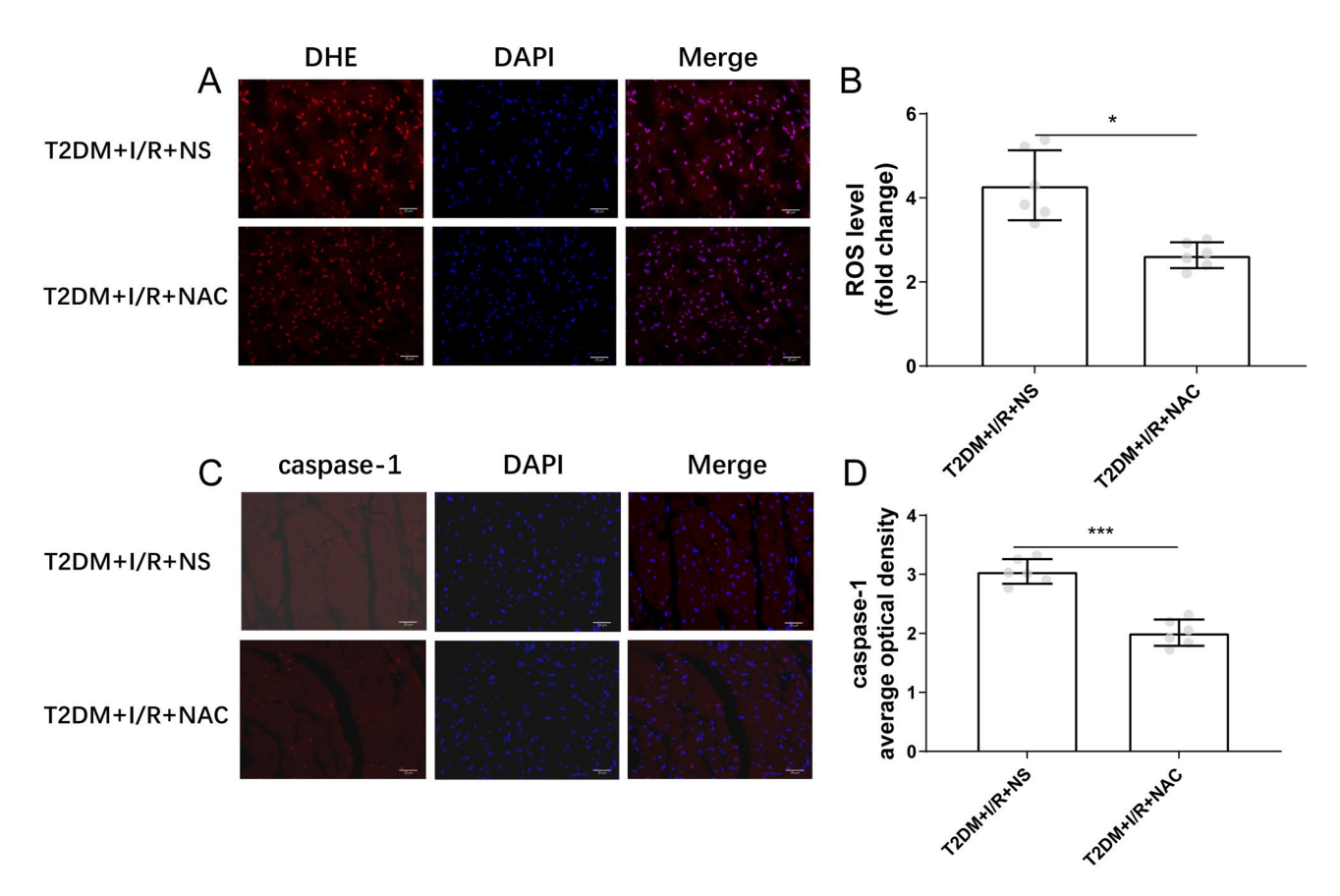


**Fig. 6.** Inhibition of ROS by N-acetylcysteine. (**A**) Rat myocardial tissue ROS immunofluorescence staining images, with red fluorescence representing ROS and blue fluorescence representing cell nuclei. (**B**) Statistical results of relative ROS fluorescence intensity in rat myocardial tissue. (**C**) Rat myocardial tissue caspase-1 immunofluorescence staining images, with red fluorescence representing caspase-1 and blue fluorescence representing cell nuclei. (**D**) Statistical results of relative caspase-1 fluorescence intensity in rat myocardial tissue. \*P < 0.05, \*\*\*P < 0.001.

oxidative stress, impairs oxidative phosphorylation metabolism, and ultimately induces cell death  $^{36}$ . Research indicates that ROS buildup and mitochondrial impairment serve as pivotal cues for the initiation of caspase-1-mediated cell pyroptosis. ROS can directly instigate NLRP3 inflammasome assembly and activation, fostering caspase-1-driven cell pyroptosis. Moreover, mitochondrial damage releases mtDNA, activating the caspase-1/GSDMD/IL-1 $\beta$ , IL-18 pathway. During myocardial ischemia/reperfusion (I/R), substantial ROS release due to myocardial damage fosters caspase-1-associated cell pyroptosis, exacerbating ischemic injury. This investigation identified T2DM and myocardial I/R as key instigators of ROS accumulation and mitochondrial damage in rat myocardial cells. Relative to the Nor+S group, T2DM+S and Nor+I/R group rats exhibited heightened ROS fluorescence intensity and mitochondrial scores in myocardial tissue. The caspase-1/GSDMD/IL-1 $\beta$ , IL-18 pathway activated within the myocardium of T2DM+S and Nor+I/R group rats. Subsequent to I/R treatment in T2DM rats, increased ROS production and aggravated mitochondrial damage in myocardial cells amplified caspase-1-dependent cell pyroptosis and the ensuing inflammatory response. This likely underpins the heightened myocardial injury observed in T2DM+I/R group rats in comparison to Nor+I/R group rats.

In our study, Fig. 5F showed elevated pro-caspase levels in the DMSO-treated group without reaching statistical significance. This result can be attributed to several factors. First, the use of DMSO as a solvent may influence cellular physiology due to its biological activity, potentially interfering with intracellular signaling pathways and causing variability in pro-caspase levels<sup>37</sup>. This interference, while visually apparent, may not manifest as statistically significant differences. Second, biological variability among experimental animals could contribute to inconsistent results. Individual differences in the animal model may affect parameter variations between treatment groups, leading to high variability within groups<sup>38</sup>. Third, the sensitivity and specificity of the detection method used in this study might have limitations, especially in detecting subtle changes, which could result in non-significant statistical outcomes despite apparent differences. Finally, the biological mechanisms underlying the observed elevated pro-caspase levels in the DMSO-treated group require further investigation. DMSO might indirectly increase pro-caspase levels by affecting inflammatory pathways or apoptosis mechanisms<sup>39</sup>. Further studies are needed to elucidate these potential mechanisms and confirm the specific effects of DMSO on caspase activity and cell apoptosis.

N-acetylcysteine (NAC) is a well-established antioxidant renowned for its efficacy in neutralizing diverse reactive oxygen species (ROS), encompassing hydrogen peroxide, hydroxyl radicals, and hypochlorous acid. Its clinical utility in treating various ailments has garnered recognition over several decades. Earlier investigations

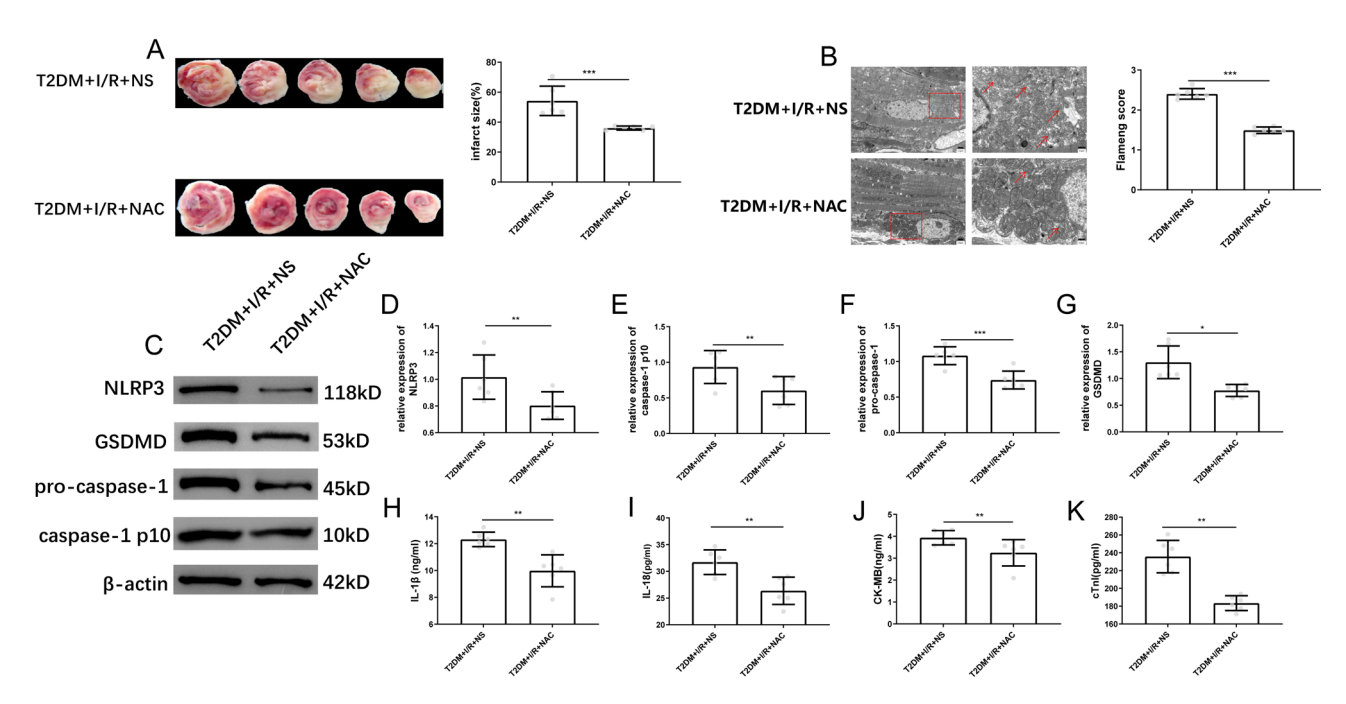


Fig. 7. Inhibit ROS-induced cell apoptosis on myocardial injury in T2DM rats following CPB ischemia–reperfusion. (A) Comparison of myocardial infarction areas between the NAC treatment group and the non-treatment group in rats. (B) Transmission electron micrograph of cardiac tissue, with the enlarged view of the red-framed area on the left shown on the right side. The arrows indicate damaged mitochondria, and statistical results of myocardial mitochondrial scoring. (C) Representative Western blot bands of apoptosis-related proteins. (D–G) Statistical results of expression levels for each apoptosis-related protein. (H–K) Statistical results of ELISA measurements for IL-1 $\beta$ , IL-1 $\beta$ , CK-MB and cTnI levels. \*P<0.05, \*\*P<0.01, \*\*\*P<0.001.

have evidenced that continuous pre-ischemia infusion or infusion within 5 min before reperfusion of NAC notably mitigates ischemia/reperfusion (I/R)-induced myocardial injury, surpassing the efficacy of an equivalent dose of NAC administered through rapid intravenous injection 30 min before ischemia. In this study, we adopted continuous tail vein infusion of NAC and substantiated its efficacy via ROS immunofluorescence. The T2DM+I/R+NAC group exhibited considerably diminished relative ROS fluorescence intensity within rat myocardium in comparison to the T2DM+I/R+NS group, signifying abated oxidative stress-induced damage. Moreover, NAC administration significantly ameliorated I/R-triggered myocardial injury, as evidenced by marked reductions in myocardial infarct size and the release of cardiac biomarkers CK-MB and cTnI. Additionally, NAC treatment markedly downregulated the expression of NLRP3, pro-caspase-1, caspase-1 p10, and GSDMD. This correlated with diminished release of IL-1 $\beta$  and IL-1 $\beta$ , hinting at a potential association between elevated cell death-associated molecules and heightened ROS production due to oxidative stress. NAC treatment partially hindered ROS-mediated activation of caspase-1-driven cell death, potentially contributing to the attenuation of myocardial and reperfusion injury. Collectively, these outcomes underscore NAC infusion as a promising therapeutic avenue for curtailing myocardial injury in the context of I/R.

This study possesses several limitations. Firstly, it solely investigates the role of cell necroptosis in animal models, omitting an examination of conventional cellular-level morphological shifts associated with necroptosis. Secondly, it solely examines short-term alterations in myocardial cell ultrastructure and necroptosis-related protein activation within T2DM rats. This study refrains from conducting extended observations and comparisons, which could offer deeper insights into the impact of T2DM-induced cell necroptosis on cardiac health and its underlying mechanisms. Thirdly, due to model constraints, the assessment of rats' cardiac function during the CPB process lacks ultrasound evaluation. Such an approach would have enhanced comprehension of cardiac functional changes and their correlation with cell necroptosis. Thirdly, the study does not comprehensively analyze necroptosis-related pathways, thus limiting our grasp of pathway interactions and mutual constraints. Lastly, although pentobarbital is commonly used in extracorporeal circulation myocardial protection studies due to its effectiveness in maintaining stable anesthesia and providing both anesthetic and analgesic effects in rodents, it does not fully replicate the complex, multi-agent anesthesia regimens (such as fentanyl, midazolam, sevoflurane) used in clinical cardiopulmonary bypass (CPB) procedures. It is important to adopt anesthesia protocols that closely mimic clinical conditions to enhance the translational potential of preclinical findings. Therefore, future studies should aim to incorporate anesthetic regimens that are more aligned with clinical practices.

To conclude, this investigation establishes that T2DM heightens myocardial necroptosis during CPB, concomitant with the activation of caspase-1-dependent cell pyroptosis. The elevation of cell death-related molecules potentially links to heightened ROS production arising from oxidative stress. NAC, functioning as an antioxidant, exhibits partial restraint over caspase-1-dependent cell death activation mediated by ROS. This intervention consequently ameliorates myocardial injury induced by I/R (Fig. 8). The findings underscore the therapeutic potential of targeting necroptosis-related pathways to safeguard against myocardial injury during CPB in T2DM patients.

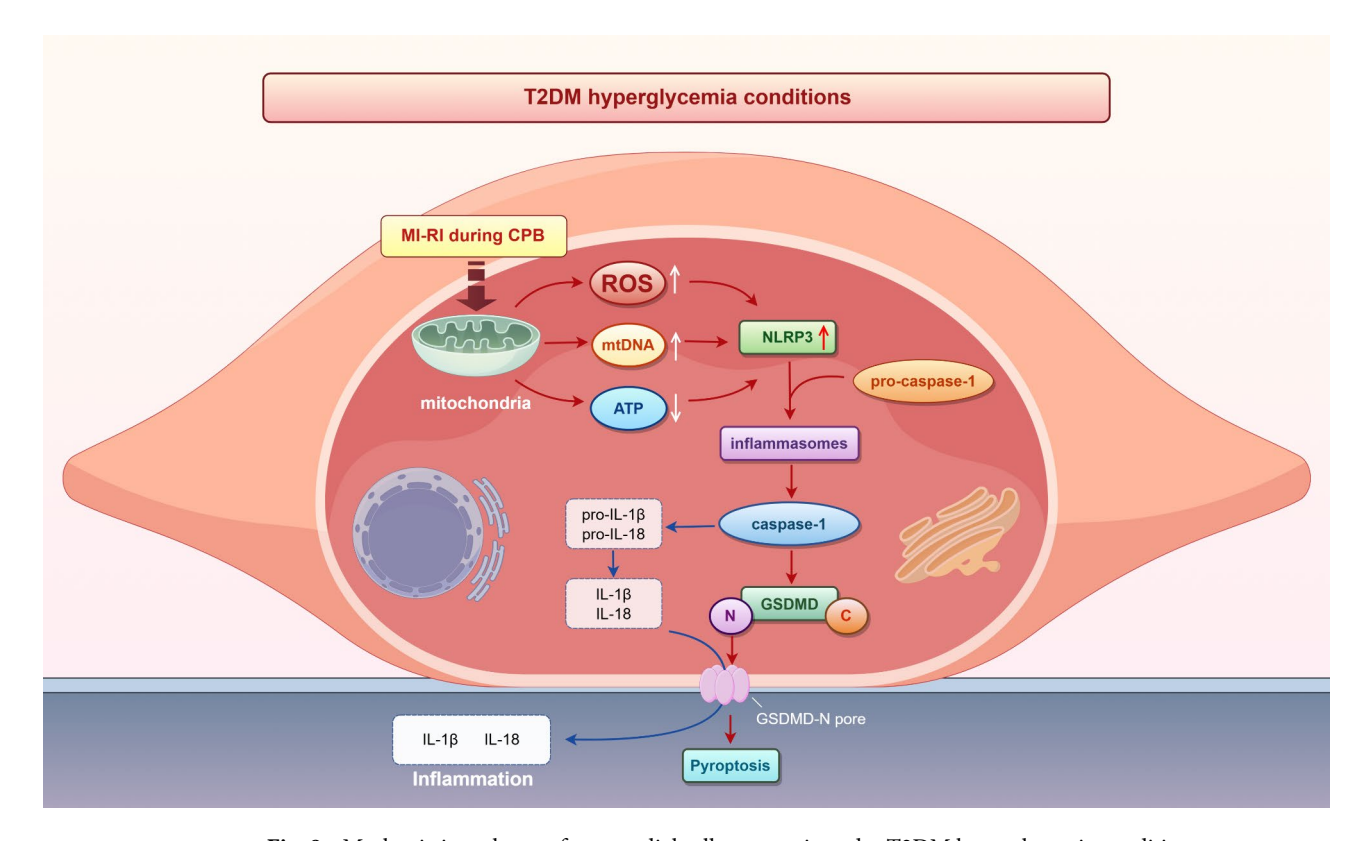


Fig. 8. Mechanistic pathway of myocardial cell pyroptosis under T2DM hyperglycemia conditions. Hyperglycemia conditions associated with T2DM exacerbate myocardial ischemia–reperfusion injury (MI-RI) occurring during CPB, leading to mitochondrial dysfunction. The dysfunction of mitochondria results in an increase in reactive oxygen species (ROS) and the release of mitochondrial DNA (mtDNA). These mitochondrial-derived signals activate the NLRP3 inflammasome, a critical component in the pyroptosis pathway. The activation of NLRP3 subsequently leads to the conversion of pro-caspase-1 into active caspase-1. Activated caspase-1 cleaves gasdermin D (GSDMD), producing its N-terminal (N) and C-terminal (C) domains. The N-terminal domain of GSDMD forms pores in the cell membrane, facilitating pyroptosis. Concurrently, caspase-1 processes pro-inflammatory cytokines, pro-IL-1 $\beta$  and pro-IL-18, into their mature forms, IL-1 $\beta$  and IL-18. The formation of GSDMD-N pores culminates in pyroptosis, characterized by cell swelling and lysis, thereby releasing IL-1 $\beta$  and IL-18 into the extracellular space and promoting inflammation. T2DM, Type 2 Diabetes Mellitus; MI-RI, Myocardial Ischemia–Reperfusion Injury; CPB, Cardiopulmonary Bypass; ROS, Reactive Oxygen Species; mtDNA, Mitochondrial DNA; NLRP3, NOD-like receptor family pyrin domain-containing 3; GSDMD, Gasdermin D; IL-1 $\beta$ , Interleukin-1 beta; IL-18, Interleukin-18.

#### Data availability

The datasets used and/or analysed during the current study available from the corresponding author on reasonable request.

Received: 13 March 2024; Accepted: 16 August 2024

Published online: 21 August 2024

#### References

- 1. Cho, N. H. et al. IDF Diabetes Atlas: Global estimates of diabetes prevalence for 2017 and projections for 2045. Diabetes Res. Clin. Pract. 138, 271–281. https://doi.org/10.1016/j.diabres.2018.02.023 (2018).
- Balakumar, P. & Sharma, N. K. Healing the diabetic heart: Does myocardial preconditioning work?. Cell. Signal. 24, 53–59. https://doi.org/10.1016/j.cellsig.2011.09.007 (2012).
- 3. Milazzo, V. et al. Diabetes mellitus and acute myocardial infarction: Impact on short and long-term mortality. Adv. Exp. Med. Biol. 1307, 153–169. https://doi.org/10.1007/5584\_2020\_481 (2021).
- 4. Iannantuoni, F. et al. Does glycemic control modulate the impairment of NLRP3 inflammasome activation in type 2 diabetes?. Antioxid. Redox Signal. 30, 232–240. https://doi.org/10.1089/ars.2018.7582 (2019).
- 5. Szpigel, A. *et al.* Lipid environment induces ER stress, TXNIP expression and inflammation in immune cells of individuals with type 2 diabetes. *Diabetologia* **61**, 399–412. https://doi.org/10.1007/s00125-017-4462-5 (2018).
- Lejay, A. et al. Ischemia reperfusion injury, ischemic conditioning and diabetes mellitus. J. Mol. Cell. Cardiol. 91, 11–22. https://doi.org/10.1016/j.yjmcc.2015.12.020 (2016).
- 7. Fu, Y., Zhou, J. D., Sang, X. Y. & Zhao, Q. T. Gualou-Xiebai-Banxia decoction protects against type II diabetes with acute myocardial ischemia by attenuating oxidative stress and apoptosis via PI3K/Akt/eNOS signaling. *Chin. J. Nat. Med.* 19, 161–169. https://doi.org/10.1016/S1875-5364(21)60017-1 (2021).

- Sun, A. et al. Mitochondrial aldehyde dehydrogenase 2 plays protective roles in heart failure after myocardial infarction via suppression of the cytosolic JNK/p53 pathway in mice. J. Am. Heart Assoc. 3, e000779. https://doi.org/10.1161/JAHA.113.000779 (2014).
- 9. Shi, J., Gao, W. & Shao, F. Pyroptosis: Gasdermin-mediated programmed necrotic cell death. *Trends Biochem. Sci.* 42, 245–254. https://doi.org/10.1016/j.tibs.2016.10.004 (2017).
- Kepp, O., Galluzzi, L., Zitvogel, L. & Kroemer, G. Pyroptosis—a cell death modality of its kind?. Eur. J. Immunol. 40, 627–630. https://doi.org/10.1002/eji.200940160 (2010).
- Jia, C. et al. Role of pyroptosis in cardiovascular diseases. Int. Immunopharmacol. 67, 311–318. https://doi.org/10.1016/j.intimp. 2018.12.028 (2019).
- He, Z. et al. Neural progenitor cell pyroptosis contributes to Zika virus-induced brain atrophy and represents a therapeutic target. Proc. Natl. Acad. Sci. U.S.A. 117, 23869–23878. https://doi.org/10.1073/pnas.2007773117 (2020).
- Sun, X., Zhou, R., Lei, Y., Hu, J. & Li, X. The ligand-gated ion channel P2X7 receptor mediates NLRP3/caspase-1-mediated pyroptosis in cerebral cortical neurons of juvenile rats with sepsis. *Brain Res.* 1748, 147109. https://doi.org/10.1016/j.brainres.2020. 147109 (2020).
- 14. Huang, D., Gao, W., Zhong, X. & Ge, J. NLRP3 activation in endothelia promotes development of diabetes-associated atherosclerosis. *Aging* 12, 18181–18191. https://doi.org/10.18632/aging.103666 (2020).
- Li, Y. et al. VX-765 attenuates atherosclerosis in ApoE deficient mice by modulating VSMCs pyroptosis. Exp. Cell Res. 389, 111847. https://doi.org/10.1016/j.yexcr.2020.111847 (2020).
- Rong, J. et al. Anti-inflammatory effect of up-regulated microRNA-221-3p on coronary heart disease via suppressing NLRP3/ ASC/pro-caspase-1 inflammasome pathway activation. Cell Cycle 19, 1478–1491. https://doi.org/10.1080/15384101.2020.17545 62 (2020)
- 17. Qiu, Z. et al. NLRP3 inflammasome activation-mediated pyroptosis aggravates myocardial ischemia/reperfusion injury in diabetic rats. Oxid. Med. Cell. Longevity 2017, 9743280. https://doi.org/10.1155/2017/9743280 (2017).
- Shi, C. et al. Diabetes induces hepatocyte pyroptosis by promoting oxidative stress-mediated NLRP3 inflammasome activation during liver ischaemia and reperfusion injury. Ann. Transl. Med. 8, 739. https://doi.org/10.21037/atm-20-1839 (2020).
- Han, Y. et al. Reactive oxygen species promote tubular injury in diabetic nephropathy: The role of the mitochondrial ros-txnipnlrp3 biological axis. Redox Biol. 16, 32–46. https://doi.org/10.1016/j.redox.2018.02.013 (2018).
- 20. Che, H. *et al.* Melatonin exerts neuroprotective effects by inhibiting neuronal pyroptosis and autophagy in STZ-induced diabetic mice. *FASEB J.* **34**, 14042–14054. https://doi.org/10.1096/fj.202001328R (2020).
- An, Y. et al. Activation of ROS/MAPKs/NF-kappaB/NLRP3 and inhibition of efferocytosis in osteoclast-mediated diabetic osteoporosis. FASEB J. 33, 12515–12527. https://doi.org/10.1096/fj.201802805RR (2019).
- 22. Jia, Y. et al. Metformin protects against intestinal ischemia-reperfusion injury and cell pyroptosis via TXNIP-NLRP3-GSDMD pathway. Redox Biol. 32, 101534. https://doi.org/10.1016/j.redox.2020.101534 (2020).
- 23. Wannamaker, W. et al. (S)-1-((S)-2-[1-(4-amino-3-chloro-phenyl)-methanoyl]-amino-3,3-dimethyl-butanoyl)-pyrrolidine-2-carboxylic acid ((2R,3S)-2-ethoxy-5-oxo-tetrahydro-furan-3-yl)-amide (VX-765), an orally available selective interleukin (IL)-converting enzyme/caspase-1 inhibitor, exhibits potent anti-inflammatory activities by inhibiting the release of IL-1beta and IL-18. J. Pharmacol. Exp. Therapeut. 321, 509–516. https://doi.org/10.1124/jpet.106.111344 (2007).
- 24. Kristiansen, S. B. *et al.* Impact of hyperglycemia on myocardial ischemia-reperfusion susceptibility and ischemic preconditioning in hearts from rats with type 2 diabetes. *Cardiovasc. Diabetol.* **18**, 66. https://doi.org/10.1186/s12933-019-0872-7 (2019).
- 25. Hu, L. et al. Targeting mitochondrial dynamics by regulating Mfn2 for therapeutic intervention in diabetic cardiomyopathy. Theranostics 9, 3687–3706. https://doi.org/10.7150/thno.33684 (2019).
- 26. Liu, W. et al. Spironolactone protects against diabetic cardiomyopathy in streptozotocin-induced diabetic rats. J. Diabetes Res. 2018, 9232065. https://doi.org/10.1155/2018/9232065 (2018).
- Pinti, M. V. et al. Mitochondrial dysfunction in type 2 diabetes mellitus: An organ-based analysis. Am. J. Physiol. Endocrinol. Metabol. 316, E268–E285. https://doi.org/10.1152/ajpendo.00314.2018 (2019).
- 28. Wang, F. et al. Silica nanoparticles induce pyroptosis and cardiac hypertrophy via ROS/NLRP3/Caspase-1 pathway. Free Radical Biol. Med. 182, 171–181. https://doi.org/10.1016/j.freeradbiomed.2022.02.027 (2022).
- 29. Zheng, J., Hu, Q., Zou, X., Xu, G. & Cao, Y. Uranium induces kidney cells pyroptosis in culture involved in ROS/NLRP3/caspase-1 signaling. Free Radical Res. 56, 40–52. https://doi.org/10.1080/10715762.2022.2032021 (2022).
- 30. Lamkanfi, M. Emerging inflammasome effector mechanisms. *Nat. Rev. Immunol.* 11, 213–220. https://doi.org/10.1038/nri2936 (2011).
- 31. Kang, P. T. et al. Mitochondrial complex I in the post-ischemic heart: Reperfusion-mediated oxidative injury and protein cysteine sulfonation. J. Mol. Cell. Cardiol. 121, 190–204. https://doi.org/10.1016/j.yjmcc.2018.07.244 (2018).
- 32. Bassil, F. et al. Reducing C-terminal truncation mitigates synucleinopathy and neurodegeneration in a transgenic model of multiple system atrophy. *Proc. Natl. Acad. Sci. U. S. A.* 113, 9593–9598. https://doi.org/10.1073/pnas.1609291113 (2016).
- Teng, J. F. et al. Polyphyllin VI Induces caspase-1-mediated pyroptosis via the induction of ROS/NF-kappaB/NLRP3/GSDMD signal axis in non-small cell lung cancer. Cancers 2020, 12. https://doi.org/10.3390/cancers12010193 (2020).
- 34. McKenzie, B. A. et al. Caspase-1 inhibition prevents glial inflammasome activation and pyroptosis in models of multiple sclerosis. Proc. Natl. Acad. Sci. U. S. A. 115, E6065–E6074. https://doi.org/10.1073/pnas.1722041115 (2018).
- 35. Yang, X. M. *et al.* The highly selective caspase-1 inhibitor VX-765 provides additive protection against myocardial infarction in rat hearts when combined with a platelet inhibitor. *J. Cardiovasc. Pharmacol. Therapeut.* **22**, 574–578. https://doi.org/10.1177/10742 48417702890 (2017).
- 36. Babel, R. A. & Dandekar, M. P. A review on cellular and molecular mechanisms linked to the development of diabetes complications. *Curr. Diabetes Rev.* 17, 457–473. https://doi.org/10.2174/1573399816666201103143818 (2021).
- Lamkanfi, M. & Dixit, V. M. Inflammasomes and their roles in health and disease. Annu. Rev. Cell Dev. Biol. 28, 137–161. https://doi.org/10.1146/annurev-cellbio-101011-155745 (2012).
- Kang, R. et al. Lipid peroxidation drives gasdermin d-mediated pyroptosis in lethal polymicrobial sepsis. Cell Host Microbe 24, 97–108. https://doi.org/10.1016/j.chom.2018.05.009 (2018).
- Hall, B. S. et al. Inhibition of the SEC61 translocon by mycolactone induces a protective autophagic response controlled by EIF2S1dependent translation that does not require ULK1 activity. Autophagy 18, 841–859. https://doi.org/10.1080/15548627.2021.19610 67 (2022).

#### **Acknowledgements**

This paper was supported by Zunyi science and technology plan project [zunshikeheHZ-2023-227], and was partially supported by National Natural Science Foundation of China (NSFC) under grant No. 81860062.

#### **Author contributions**

Conception and design: Haiying Wang, Wenjing Zhou Collection and assembly of data: Wenjing Zhou, Yingya Yang, Zhouheng Feng Data analysis and interpretation: Wenjing Zhou, Yingya Yang, Yiman Chen Manuscript writing: Wenjing Zhou, Yu Zhang Final approval of manuscript: All authors.

#### Competing interests

The authors declare no competing interests.

#### Additional information

**Supplementary Information** The online version contains supplementary material available at https://doi.org/10.1038/s41598-024-70477-5.

**Correspondence** and requests for materials should be addressed to H.W.

Reprints and permissions information is available at www.nature.com/reprints.

**Publisher's note** Springer Nature remains neutral with regard to jurisdictional claims in published maps and institutional affiliations.

Open Access This article is licensed under a Creative Commons Attribution-NonCommercial-NoDerivatives 4.0 International License, which permits any non-commercial use, sharing, distribution and reproduction in any medium or format, as long as you give appropriate credit to the original author(s) and the source, provide a link to the Creative Commons licence, and indicate if you modified the licensed material. You do not have permission under this licence to share adapted material derived from this article or parts of it. The images or other third party material in this article are included in the article's Creative Commons licence, unless indicated otherwise in a credit line to the material. If material is not included in the article's Creative Commons licence and your intended use is not permitted by statutory regulation or exceeds the permitted use, you will need to obtain permission directly from the copyright holder. To view a copy of this licence, visit <a href="http://creativecommons.org/licenses/by-nc-nd/4.0/">http://creativecommons.org/licenses/by-nc-nd/4.0/</a>.

© The Author(s) 2024